remote sensing

MDPI

Article

Seismogenic Source Model of the 2019, M_w 5.9, East-Azerbaijan Earthquake (NW Iran) through the Inversion of Sentinel-1 DInSAR Measurements

Emanuela Valerio [1], Mariarosaria Manzo [1], Francesco Casu [1], Vincenzo Convertito [2], Claudio De Luca [1], Michele Manunta [1], Fernando Monterroso [1,3], Riccardo Lanari [1,*] and Vincenzo De Novellis [1]

[1] Istituto per il Rilevamento Elettromagnetico dell'Ambiente, IREA-CNR, 80124 Napoli, Italy
[2] Istituto Nazionale di Geofisica e Vulcanologia, Osservatorio Vesuviano, 80124 Napoli, Italy

* Correspondence: lanari.r@irea.cnr.it;

Received: 13 March 2020; Accepted: 21 April 2020; Published: 24 April 2020

Introduction

This supplement contains supporting figures cited in the main document. In particular, it is aimed to provide additional information on:

a) Sentinel-1 DInSAR measurements (Figure S1).

b) The performance analysis relevant to the source model (Figure S2).

c) Coulomb stress change sections (Figure S3).

d) Shalgun-Yelimsi fault modelling results (Figure S4).

The availability of both ascending and descending SAR data set allows us not only to detect the ground deformation in the corresponding LOS, but also to discriminate the vertical and east–west components of the displacement [1,2]. To achieve this task, we properly combined the displacement maps computed from the ascending and descending orbits on pixels common to both maps, taking into account the different acquisition geometries at each pixel; we present in Figure S1 the achieved vertical and east–west displacement maps.

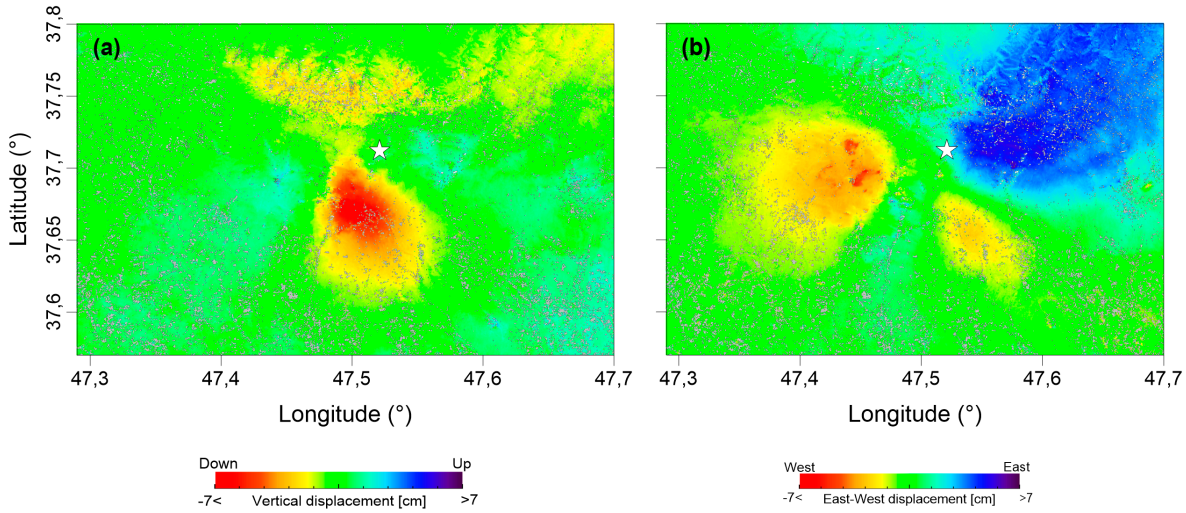

Figure S1. Sentinel-1 DInSAR measurements. (a) Vertical and (b) East-West displacements maps obtained through the combination of the geocoded displacement maps computed from the ascending and descending orbits. The vertical displacement map shows both an uplift of about 2 cm and a subsidence of about 7 cm near the epicentral zone, while the east–west displacement map clearly highlights a greater displacement to the west of more than -5 cm.

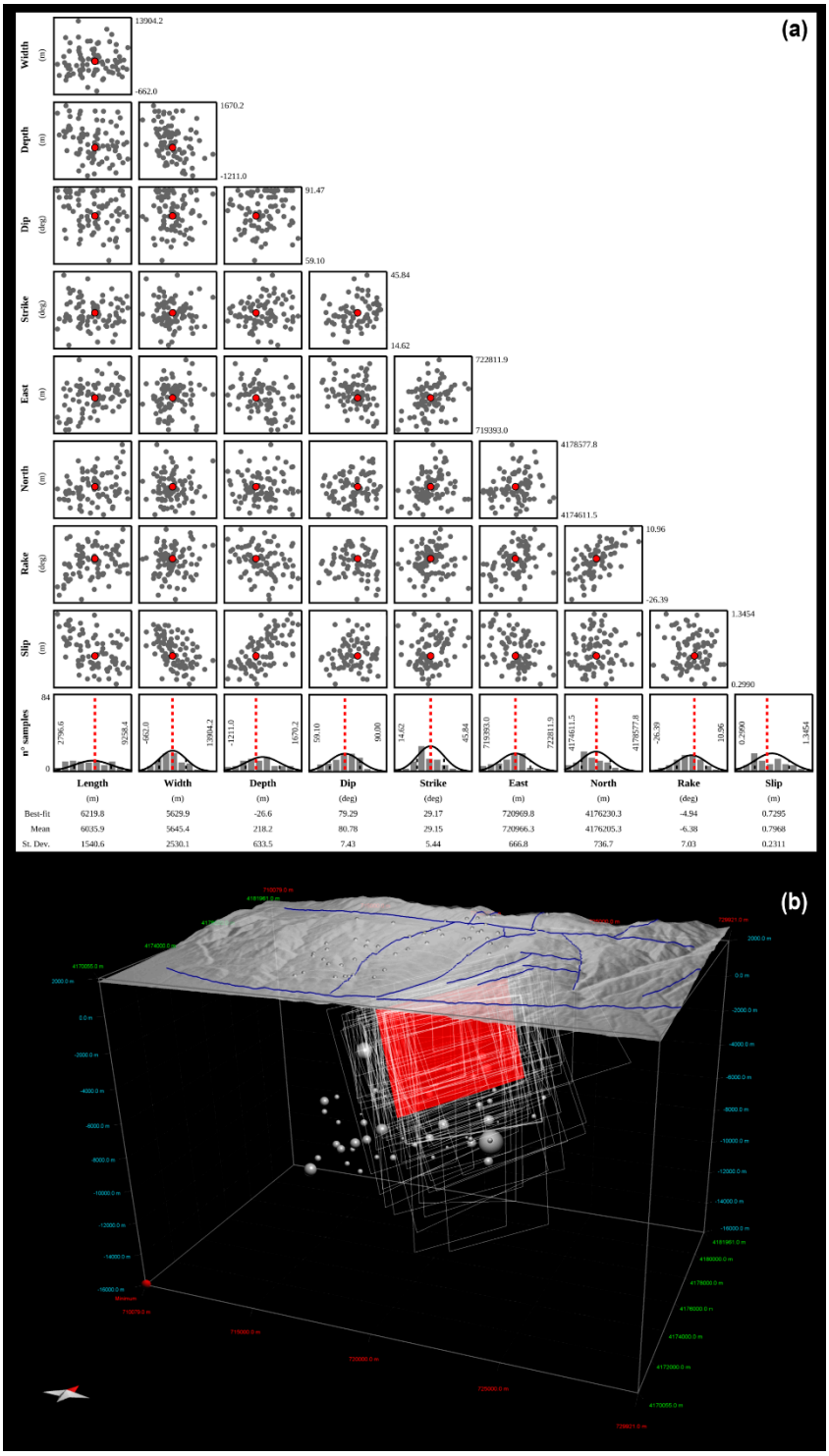

Figure S2. Performance analysis relevant to the source model. (a) Fault parameter uncertainties and trade-offs for the seismic source model of the 2019 E- Azerbaijan earthquake retrieved by Sentinel-1 measurements. Histograms show the a posteriori probability distribution of fault parameters, and scatterplots show trade-offs between parameters. Details on the estimation of these parameters can be found in [3]. (b) Three-dimensional representation of the fault plane statistics. Seismicity distribution (white spheres) recorded from 7 to 9 November 2019 is shown as a function of magnitude (the higher the magnitude, the bigger the spheres). The main local structures are also indicated with blue lines and are superimposed on the 1 arcsec Shuttle Radar Topography Mission (SRTM) Digital Elevation Model (DEM) of the zone.

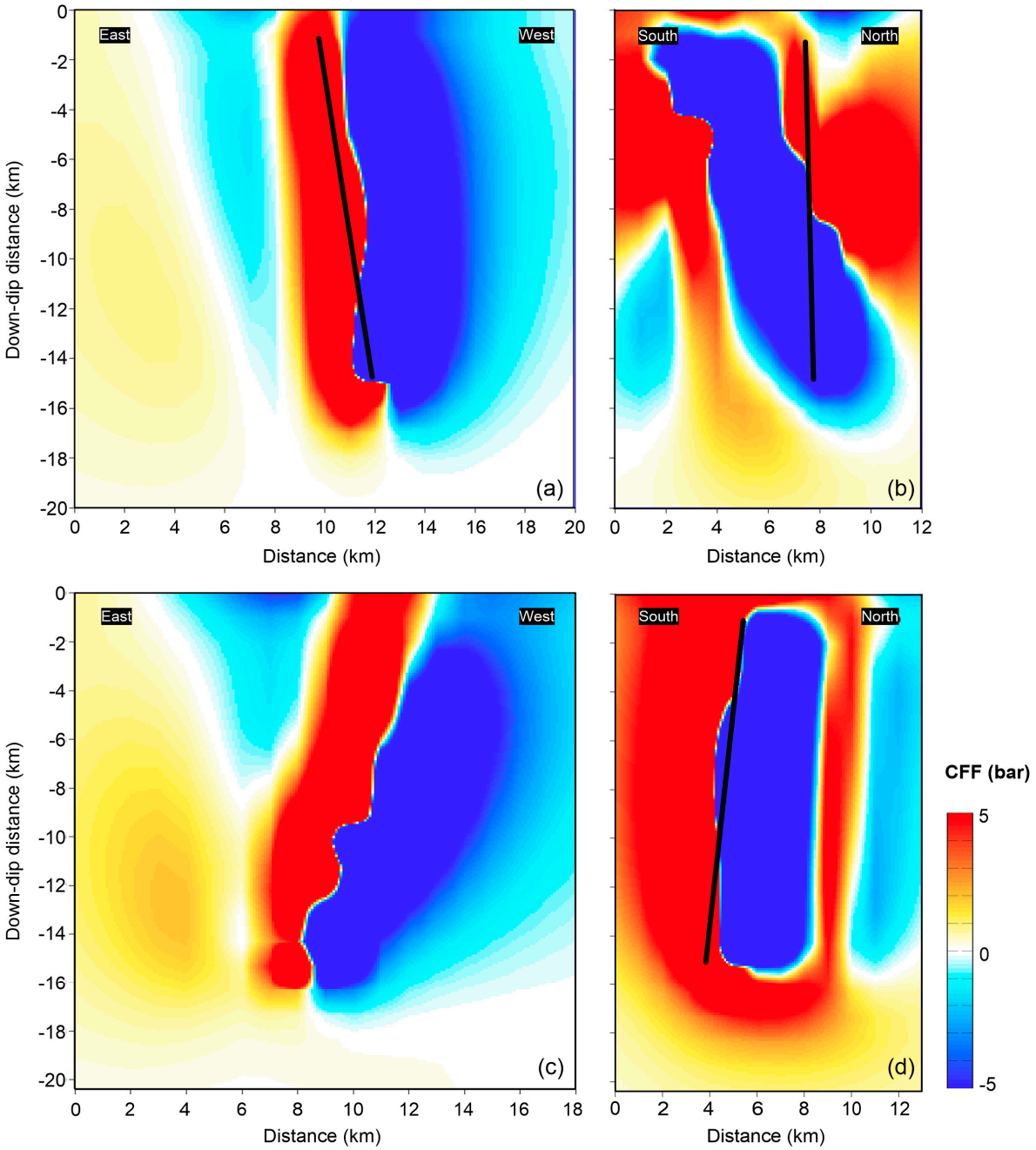

Figure S3. Coulomb stress change distribution at depth along the considered four faults: (a) F1, (b) F2, (c) F3 and (d) F4, respectively. The black line represent our fault solution; the effective friction coefficient (μ′) is equal to 0.6.

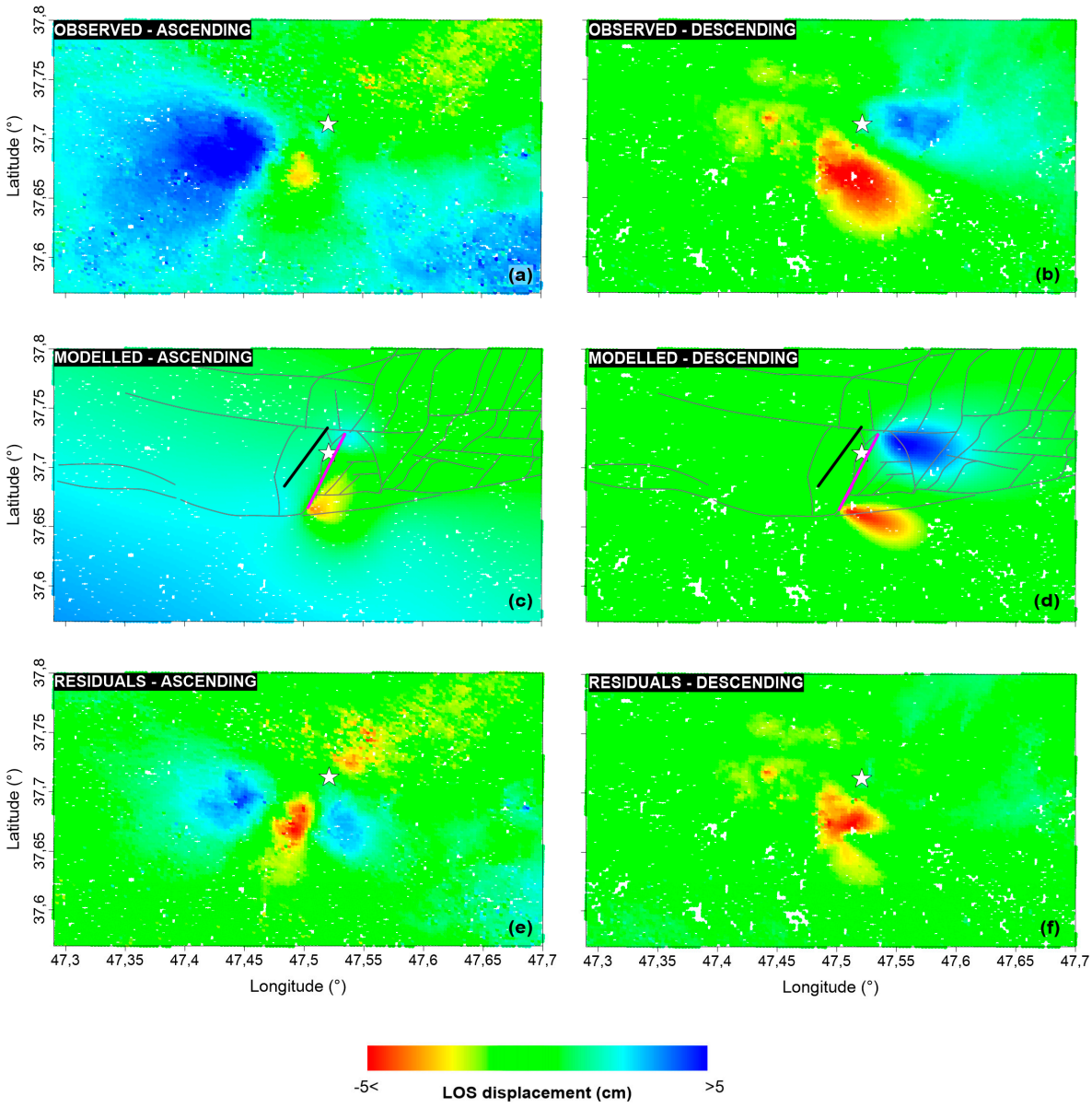

Figure S4. Shalgun-Yelimsi fault modelling results. We consider as seismogenic source a structure consistent with the reported location and orientation of the Shalgun-Yelimsi Fault [4]. LOS projected displacement maps for S1 ascending (a) and descending (b) orbits interferograms; note that they are the same of Fig. 2a and 2b and are repeated here only for sake of completness. LOS projected displacement maps computed from the retrieved analytical model for the S1 ascending (c) and descending (d) orbits interferograms reported in panels (a) and (b). Their corresponding residual maps are shown in (e) and (f), respectively. The solid magenta line indicates the retrieved fault plane solution relevant to the Shalgun-Yelimsi Fault, while the black one the fault plane solution proposed in this work and detailed in the main text. The white star and the grey lines indicate the M_w 5.9 E-Azerbaijan mainshock and the main local structures derived from [4], respectively. By comparing the maps shown in Figure S4e and S4f with those presented in Figure 3e and 3f, respectively, it is evident that the geodetic inversion of the exploited DInSAR measurements results into a best-fit solution whose residuals are significantly worse than those achieved for our preferred model.

References

1. Manzo, M., *et al.* Surface deformation analysis in the Ischia Island (Italy) based on spaceborne radar interferometry. *J. Volc. Geother. Res.* **2006**, *151*, 399-416, doi: 10.1016/j.jvolgeores.2005.09.010.
2. Casu F.; Manconi, A. Four-dimensional surface evolution of active rifting from spaceborne SAR data. *Geosphere* **2016**, doi: 10.1130/GES01225.1.
3. Atzori, S., *et al*. Finite fault inversion of DInSAR coseismic displacement of the 2009 L'Aquila earthquake (Central Italy). *Geophys. Res. Lett.* **2009**, *36*, L15305, doi: 10.1029/2009GL039293.
4. Faridi, M.; Burg, J. P.; Nazari, H.; Talebian, M.; Ghorashi, M. Active faults pattern and interplay in the Azerbaijan region (NW Iran). *Geotectonics* **2017**, *51*, 428-437, doi: 10.1134/S0016852117040033.